

1
2
3
4 **Fatigue design of lattice materials via computational mechanics:**
5
6
7 **application to lattices with smooth transitions in cell geometry**
8
9

10
11
12
13
14 **Ehsan Masoumi Khalil Abad, Sajad Arabnejad Khanoki, Damiano Pasini^{†‡}**
15

16
17
18
19 **Ehsan Masoumi Khalil Abad:** PhD candidate, Mechanical Engineering Department, McGill
20
21 University, Montreal, Quebec, Canada. Email: ehsan.masoumikhililabad@mail.mcgill.ca
22
23

24
25
26 **Sajad Arabnejad Khanoki:** PhD candidate, Mechanical Engineering Department, McGill
27
28 University, Montreal, Quebec, Canada. Email: sajad.arabnejadkhanoki@mail.mcgill.ca
29
30

31
32
33 **Damiano Pasini:** Associate Professor, Mechanical Engineering Department, McGill University,
34
35 Montreal, Quebec, Canada. Email: damiano.pasini@mcgill.ca
36
37
38
39
40
41
42
43
44
45
46
47
48
49
50
51
52
53
54
55
56
57
58

59 [†] Corresponding author. Tel: +1 514 398 6295; Fax: 514 398 7365; Email: damiano.pasini@mcgill.ca
60
61 [‡] Both PhD students were equally involved and contributed to this work.
62
63
64
65

Abstract

A numerical method based on asymptotic homogenization theory is presented for the design of lattice materials against fatigue failure. The method is applied to study the effect of unit cell shape on the fatigue strength of hexagonal and square lattices. Cell shapes with regular and optimized geometry are examined. A unit cell is considered to possess a regular shape if the geometric primitives defining its inner boundaries are joined with an arc fillet, whose radius is 1% of the cell length. An optimized cell shape, on the other hand, is obtained by minimizing the curvature of its interior borders, which are conceived as continuous in curvature to smooth stress localization.

For a given multi-axial cyclic loading, failure surfaces of metallic hexagonal and square lattices are provided along with their Modified Goodman diagrams to assess the effect of mean and alternating stresses on the fatigue strength. In good agreement with the experimental data available in literature, the numerical results show that the shape of the unit cell has a major impact on the fatigue performance of the lattice material. For example under fully reversible tension, the fatigue strength of optimized square lattices of 10% relative density is shown to be 54% higher than that of their conventional counterparts with regular cell geometry.

1. Introduction

A lattice material is a cellular material with a periodic arrangement of cells in either two or three dimensions. Besides mechanically superior to any other material [1-3], lattice materials have been shown to be attractive for their multifunctional properties, e.g. thermal insulation, sound resistance and shock energy damping, and thus to be of potential use in a broad range of applications, including battery electrodes, catalyst supports, vibration insulators, jet-engine nacelles, ultra lightweight sandwich panels, and biomedical implants, [3-8].

1
2
3
4 In several applications, the load applied to a lattice material is far from being static. The
5
6 recurring waves on a ship hull, the aero-acoustic excitation of a turbine engine, and the rhythmic
7
8 forces acting on an orthopedic implant during the swing phase of walking are all classical
9
10 examples of time-dependent loads [9-14]. A cyclic load has generally a detriment impact on the
11
12 resistance of the lattice material. Factors that govern fatigue failure are not limited to the
13
14 alternating and mean stresses, load frequency, environment conditions, and macroscopic form of
15
16 the structure, but include also the geometry of the microstructure, i.e. the geometry in which the
17
18 unit cell of the lattice is shaped. If geometric discontinuities are embedded at either the macro
19
20 or/and the micro scale, then a severe drop in the fatigue resistance is observed.
21
22
23
24

25 From literature, it appears that the study of fatigue failure in cellular materials, with both random
26
27 (foam) and periodic arrangement of cells (lattice), has received less attention than their
28
29 monotonic quasi-static and dynamic properties [8, 15-21]. Among the investigations, both
30
31 experimental and theoretical approaches have been developed for metallic and polymeric cellular
32
33 materials under fatigue conditions. The experimental works are predominant and mainly stem
34
35 from studies on foams [22-29], which aim at determining the stress-life curves under shear and
36
37 axial loadings. For example, Burman [28] experimentally characterized the fatigue behavior of
38
39 sandwich panels with polymeric PVC and PMI foam cores. The effect of the alternating strain on
40
41 the fatigue life of polymeric cellular materials was shown to be more significant than that of the
42
43 mean stress. It was also observed that reversible cyclic loadings, with negative max to min stress
44
45 ratio, drastically reduce the fatigue resistance of polymeric foams. In another work, closed-cell
46
47 aluminum alloy foams, Alulight and Alporas, were tested under alternating loads of fracture
48
49 mode I to measure their fatigue resistance to crack propagation [29]. Crack evolution was
50
51 observed to be controlled by linear elastic fracture mechanics. On the other hand, due to the high
52
53 sensitivity of the crack propagation rate to the alternating stress intensity, the conventional
54
55
56
57
58
59
60
61
62
63
64
65

1
2
3
4 damage-tolerant methodology was found to be inappropriate for use in the fatigue design of
5
6 aluminum foams. McCullough et al. [30] observed that ratcheting in closed cell Alulight foam is
7
8 the dominant cyclic deformation mode for a tension–tension and compression–compression load.
9
10 In another study on crack propagation, Motz et al. [31] experimentally showed that a cellular
11
12 solid with hollow spheres made of a stainless steel (316L) has fatigue strength 50% to 60% lower
13
14 than that of a closed cell aluminum foam. Such strength reduction was attributed to the presence
15
16 of stress concentration at the bonding points between spheres.
17
18

19
20 Studies on the fatigue of lattice materials are even less than those on foams. On the experimental
21
22 side, Côté et al. [9], among few researchers, characterized the stress-life curves of sandwich
23
24 panels with a lattice core made of stainless steel. Sandwich panels with a unit cell of diamond
25
26 shape have been observed under alternating shear weaker than under axial load. A fatigue
27
28 collapse map was generated for stainless steel sandwich beams with pyramidal core [10] and
29
30 crack nucleation sites leading to failure were identified in the micro structure. Under cycling
31
32 loading it was shown that the brazed joints are the weakest points of the panel core, hence their
33
34 effect is to significantly reduce the shear fatigue strength. In another study, Côté et al. [11]
35
36 examined the available experimental data for metallic lattice and foam cores and showed that the
37
38 fatigue to monotonic strength ratio, $\Delta \bar{\tau}_e / \tau_{ult}$, are close to 0.3 and 0.2, respectively, for R=0.1
39
40 and R=0.5. The data, gathered from a wide range of lattice cores, suggested that the fatigue to
41
42 monotonic strength ratio generally does not depend on *core topology, relative density, and*
43
44 *material properties.*
45
46
47
48
49
50
51

52
53 On the theoretical side, empirical relationships of finite/infinite life as well fracture mechanics
54
55 approaches have been employed to predict the fatigue life of a periodic cellular solid [32-34]. In
56
57 these studies, the cell walls were assumed to flex like a beam. However, as observed by Simone
58
59 et al [35], the use of beam elements, rather than continuum elements, such as plane elements, is
60
61

1
2
3
4 not appropriate to capture accurately the real stress distribution in the lattice cells. In fact, this
5
6 assumption can lead to unrealistic results that may limit the use of these methods for fatigue
7
8 design.
9

10
11 From the literature on lattice materials, it appears that most of the methods for fatigue design rely
12
13 on experiments, which are tailored to handle selected lattice topologies and materials, besides
14
15 being time consuming and often expensive. Current theoretical approaches, on the other hand,
16
17 seem to lack accuracy, since they might fail to capture the real stress distribution in the lattice
18
19 cells.
20
21

22
23 This work proposes a fatigue design methodology that can assess with accuracy the real stress
24
25 distribution in the lattice cell wall. **Since the failure mechanisms of a cellular material strongly**
26
27 **depend on the properties of the bulk solid material, we have decided here to focus our attention**
28
29 **on metallic cellular materials.** Based on computational mechanics, the method is validated
30
31 through experimental data from literature. As described in section 2, asymptotic homogenization
32
33 theory is used to computationally model the elastic-plastic behavior of the lattice, as well as
34
35 determine strength values and real stress distribution in the lattice cells. In section 3, modified
36
37 Goodman diagrams for fatigue design of planar lattices with regular geometry, i.e. cell shapes
38
39 with sharp corners, and optimized geometry, i.e. cells with smoothed inner profiles, are
40
41 generated. The maps provide insight into the impact that both alternating and mean stress have
42
43 on the fatigue life of hexagonal and square lattice cells with regular and optimized geometry.
44
45
46
47
48
49
50
51

52 **2. Fatigue design methodology**

53
54 Infinite-life, safe-life, fail-safe, and damage-tolerant criteria are well-established approaches for
55
56 the design of a material against fatigue fracture and degradation. Each method requires specific
57
58 properties to characterize the material behavior under fatigue. Certain properties, e.g. the
59
60
61

1
2
3
4 endurance limit, can be generally obtained from traditional approaches, e.g. the stress (strain)-life
5
6 method, other can determined though more recent techniques based on fracture mechanics. The
7
8 stress (strain)-life method introduced by Wholer is one approach that provides the number of
9
10 cycles that a smooth test specimen can resist under alternating stresses (strains) of constant
11
12 amplitude before fracture. The Wholer's strain-life curves help to gain insight into the influence
13
14 of the number of cycles on the alternating stress, but they fail to capture the detrimental effect of
15
16 the mean stress. For this purpose, other methods have been proposed. One of these is the
17
18 constant-life diagram (Figure 1), which is constructed by curve fitting of experimental data for
19
20 various combinations of stress amplitudes and mean stresses. Goodman, Soderberg, Gerber, and
21
22 modified Goodman are the most common curve fitting models.
23
24
25
26

27
28 In this work, we develop the modified Goodman diagrams for lattice materials [36] under high
29
30 cycle fatigue loading. We assume the specimen to be free of damage, since the endurance limit is
31
32 very sensitive to the specimen conditions, such as scratches, notches and nicks [36]. As shown in
33
34 Figure 1, the material properties necessary to generate the diagram are: yield strength, ultimate
35
36 strength and fatigue strength for a given life, or endurance limit for materials with infinite life.
37
38 Once these properties are determined, the diagram can be constructed (Figure 1) from the
39
40 intersection of i) the line connecting the material ultimate and fatigue strengths for a given life
41
42 with ii) a 45° degree sloped line, originated from the monotonic yield strength of the material.
43
44
45
46
47

48 To extend the application of the modified Goodman model to planar lattice materials, we assume
49
50 the reference lattice material be free of defects. We also assume that the cell wall material is a
51
52 continuum media with properties comparable to those of its bulk material, which means that the
53
54 material has one level of structural hierarchy. This hypothesis sets the limit of applicability of the
55
56 proposed method to a minimum length-scale that depends on the material microstructure, slip
57
58 system, grain and size [37-39]. If the effect of nanostructure defects, grain and size of the
59
60
61
62
63
64
65

1
2
3
4 material, has to be modeled, then two length scales in the lattice microstructure should be
5
6 considered, as described by Zienkiewicz and Taylor [40].
7

8
9 Next section describes how to obtain the properties required to generate the modified Goodman
10
11 diagram. For this purpose, asymptotic homogenization theory, one among other homogenization
12
13 approaches [2, 4, 15, 21, 41], is chosen here and implemented in a computational framework,
14
15 since its mathematical foundation has been proved together with its capacity to accurately
16
17 capture the real stress distribution within the cell walls of a lattice.
18
19

20 21 22 **2.1 Homogenized strength of lattice materials**

23
24 The analysis of a lattice material is often performed by isolating a representative volume element
25
26 (RVE) and calculating its properties, which under certain assumptions represent the
27
28 homogenized properties of the macro material. Theoretical, numerical, and experimental
29
30 approaches can be used to homogenize the properties of a lattice [2, 15, 16, 42-52]. Here, we use
31
32 asymptotic homogenization to determine its effective mechanical properties, including the
33
34 effective stiffness, yield and ultimate strength. Besides the linear elastic terms [53, 54], we model
35
36 also the effect of material non-linearity as a result of plastic deformation [55, 56]. Asymptotic
37
38 homogenization allows obtaining the macroscopic stresses that lead to the microscopic yield, or
39
40 fracture, as well as the endurance limit of the lattice. While in this work the method is
41
42 demonstrated with reference to two common loadings, i.e. in-plane uni-axial and pure shear
43
44 loadings, yield surfaces are also provided for the fatigue design of lattice materials under any
45
46 combination of load.
47
48
49
50
51

52
53 The underlying assumption of asymptotic homogenization is that each field quantity depends on
54
55 two different scales: one on the macroscopic level x , and the other on the microscopic level,
56
57 $y=x/\varepsilon$, where ε is a magnification factor that scales the dimensions of a unit cell to those of the
58
59
60
61

material at the macroscale. In addition, the field quantities, such as displacement, stress, and strain are considered periodic at the microscale and assumed to vary smoothly at the macroscopic level [47, 53].

Under the assumption of small deformation, the standard weak form of the equilibrium equations for a cellular body Ω^ε with the pertinent geometrical details of voids and cell wall is by [53]

$$\int_{\Omega^\varepsilon} \{\varepsilon^0(v) + \varepsilon^1(v)\}^T [E] \{\bar{\varepsilon}(u) + \varepsilon^*(u)\} d\Omega^\varepsilon = \int_{\Gamma_t} \{t\}^T \{v\} d\Gamma \quad (1)$$

where $[E]$ is the local elasticity tensor that depends on the position within the RVE, $\{\varepsilon^0(v)\}$ and $\{\varepsilon^1(v)\}$ are the virtual macroscopic and microscopic strains, respectively, $\{\bar{\varepsilon}(u)\}$ is the average or macroscopic strain, $\{\varepsilon^*(u)\}$ is the fluctuating strain varying periodically at the microscale level, and $\{t\}$ is the traction at the traction boundary Γ_t . Being the virtual displacement, $\{v\}$ may be chosen to vary only on the microscopic level and be constant on the macroscopic level.

Based on this assumption, the microscopic equilibrium equation can be obtained as

$$\int_{\Omega^\varepsilon} \{\varepsilon^1(v)\}^T [E] \{\bar{\varepsilon}(u) + \varepsilon^*(u)\} d\Omega^\varepsilon = 0 \quad (2)$$

Taking the integral over the RVE volume (V_{RVE}), equation (2) may be rewritten as

$$\int_{V_{RVE}} \{\varepsilon^1(v)\}^T [E] \{\varepsilon^*(u)\} dV_{RVE} = - \int_{V_{RVE}} \{\varepsilon^1(v)\}^T [E] \{\bar{\varepsilon}(u)\} dV_{RVE} \quad (3)$$

The above equation represents a local problem defined on the RVE. For a given applied macroscopic strain, the material can be characterized if the fluctuating strain, $\{\varepsilon^*(u)\}$, is known.

The periodicity of the strain field is ensured by imposing periodic boundary conditions on the RVE edges (figure 2); the nodal displacements on the opposite edges are set to be equal [53, 57]. equation (3) can be discretized and solved via finite element analysis as described in [46, 53-55].

For this purpose, equation 3 can be simplified to obtain a relation between the microscopic displacement field $\{D\}$ and the force vector $\{f\}$ as

$$[K]\{D\} = \{f\} \quad (4)$$

where $[K]$ is the global stiffness matrix defined as

$$[K] = \sum_{e=1}^m [k^e], [k^e] = \int_{Y^e} [B]^T [E_t][B] dY^e \quad (5 \text{ a,b})$$

being $\sum_{e=1}^m (\cdot)$ the finite element assembly operator, m the number of elements, $[B]$ the strain-displacement matrix, $[E_t]$ the tangent modulus of the elastic-plastic bulk material, and Y^e the element volume. The force vector $\{f\}$ in equation 4 is expressed as

$$\{f\} = \sum_{e=1}^m \{f^e\}, \{f^e\} = \int_{Y^e} [B][E_t]\{\bar{\varepsilon}(u)\} dY^e \quad (6)$$

It is interesting to note that $\{\bar{\varepsilon}(u)\}$ in equation 6 describes the initial strain field applied to each element of the unit cell. As a result, the force vector $\{f\}$ is a function not only of the applied strain but also of the properties of the solid material. Since in this work plastic deformation is required to determine fatigue strength, equation (4) can be considered as a system of non-linear equations that can be solved with the Newton-Raphson scheme. As shown in figure 3, the computational analysis is accomplished by imposing increments of macroscopic strain, as described in plastic theory [58, 59]. While the macroscopic strain $\{\Delta \bar{\varepsilon}(u)\}$ is increased monotonically, the force vector increment is computed and replaced in equation (4) to evaluate the displacement field. During the procedure (right hand side of Fig. 3), the effective material coefficients are kept constant until the stress reaches the yield strength of the base material. The mechanical properties of the yielded elements are replaced, iteratively, with the tangent modulus

1
2
3
4 of the elastic–plastic bulk material [58, 59]. Once the displacement field is obtained, the
5
6 fluctuating strain $\{\Delta \varepsilon^*(u)\}$ is determined by the product of the strain-displacement matrix, $[B]$,
7
8
9 and the nodal displacement vector. The increment of the microscopic strain is then determined
10
11 through the equation:

$$\{\Delta \varepsilon(u)\} = \{\Delta \bar{\varepsilon}(u)\} + \{\Delta \varepsilon^*(u)\} \quad (7)$$

12
13
14
15
16
17 The stress field in the unit cell is updated with respect to the elastic strain, and the stress average
18
19 is computed over the unit cell to attain the effective macroscopic strength as:

$$\{\bar{\sigma}\} = \frac{1}{|V_{RVE}|} \int_{V_{RVE}} \{\sigma(u)\} dV_{RVE} \quad (8)$$

20
21
22
23
24
25
26
27 The macroscopic stress, Eq. (8), represents either the yield $\{\bar{\sigma}_y\}$ or the ultimate $\{\bar{\sigma}_{ult}\}$ strength
28
29 of the unit cell when the stress level at any local point of the microstructure reaches respectively
30
31 the yield or ultimate strength of the solid material. The whole procedure, which includes the
32
33 generation of the model and its mesh, as well as the nonlinear plasticity analysis, has been
34
35 implemented into ANSYS (Canonsburg, Pennsylvania, U.S.A), where the von Mises yield
36
37 criterion with the associated flow rule has been considered for plasticity analysis.
38
39

40
41
42 Since for a high cycle fatigue failure, as it is considered in this work, the stress level is lower
43
44 than the yield of the bulk material, the linear elasticity assumption holds. Hence, the fatigue
45
46 strength of the unit cell can be obtained through the product of the unit cell yield strength with
47
48 the ratio of the endurance limit to yield strength of the bulk material as:
49
50

$$\{\bar{\sigma}_e\} = \{\bar{\sigma}_y\} \frac{\sigma_e}{\sigma_y} \quad (9)$$

51
52
53 where σ_y and σ_e are respectively the yield strength and the endurance limit of the bulk
54
55 material, and $\{\bar{\sigma}_e\}$ is the endurance limit of the unit cell. These properties are required to
56
57
58
59
60
61
62
63
64
65

1
2
3
4 construct the modified Goodman diagram (Figure 1) for any type of cell topology, as shown in
5
6 the next section.

9 **3. Cell geometries under investigation**

10
11 Square and hexagon are here selected as representative shapes of the unit cell. Since for a given
12
13 cell geometry the shape of the cell has a significant effect on the static and fatigue properties of
14
15 the lattice material [60-62], we examine regular and optimized shapes for square and hexagonal
16
17 lattices. As shown in the flowchart of Fig. 3, the methodology to obtain the fatigue properties of
18
19 the optimized cell geometry consists of three integrated parts that combine notions of design
20
21 optimization and asymptotic homogenization theory. First, the shape synthesis of the unit cell is
22
23 carried out to obtain a cell free of stress concentration (details given below); then its fatigue
24
25 properties are computed to generate the modified Goodman diagram at given relative densities;
26
27 the last step involves the minimization of the von Mises stress in the cell wall.
28
29
30
31
32

33 For square and hexagonal lattices, we study cell shapes with the following characteristics:

- 34
35 1. *G^1 cells with sharp corners.* These cells represent a conventional lattice with regular cell
36
37 geometry. The fillets at the cell joints are specified by an arc with radius equal to 1% of the
38
39 RVE length, which is representative of a sharp fillet resulting from a given manufacturing
40
41 process. The choice of the small-arc fillet enables to obtain a realistic material distribution in
42
43 a cell member [35], approximately similar to that measured through experiments [10, 11].
44
45 These cells are named here G^1 , where G represents “geometry” and the superscript shows the
46
47 degree of continuity of the geometry. As seen in figure 4, G^1 cells have continuous tangent
48
49 along their inner boundary profile, but the curvature at the blending points between the
50
51 straight and arc geometric primitives is discontinuous.
52
53
54
55
56
- 57
58 2. *G^1 cells with optimum fillet radius.* The G^1 cells with sharp corners are here optimized to
59
60 obtain a value of the fillet radius that reduces the effect of stress concentration. A classical
61
62
63
64
65

1
2
3
4 optimization problem is formulated with the objective of minimizing the maximum value of
5
6 the microscopic von Mises stress in the lattice under a given loading. The fillet radius and the
7
8 thickness at the middle of the struts (Figure 4) are considered as interdependent design
9
10 variables. A design constraint is set on the relative density. The problem is solved by
11
12 implementing a conjugate gradient method. For given relative density and design variables a
13
14 unique solution is found, as described in section 5.
15
16
17

18 **3. G^2 cell with continuous optimum curvature of the fillet.** The inner profile of these unit cells
19
20 are here synthesized through a methodology recently introduced to obtain lattice structures
21
22 free of stress-concentration [63]. The method is based on a well-known engineering theory
23
24 stating that the stress concentration due to the presence of curvature discontinuity in a
25
26 component has the effect of localizing high peak of stress [64]. Thus, synthesizing the inner
27
28 boundary of a cell with curves that are continuous in their curvature, i.e. G^2 -continuous curves
29
30 [65], improves the fatigue and monotonic strengths of the lattice. Furthermore, to avoid high
31
32 bending moments caused by curved cell members, the cell walls can be designed to be *as*
33
34 *straight as possible*, i.e. with the smallest possible curvature. The top left quadrant of Figure
35
36 3 shows the optimization formulation used in this study, while the details are given in [63].
37
38 Figure 5 (a-b) shows the parametric view of square and hexagonal cells, whose G^2
39
40 continuous profiles of their inner profiles are optimized with minimum curvature. **Besides**
41
42 **curvature minimization, a step of size optimization follows the computational analysis of the**
43
44 **yield strength (Figure 3). Here, the wall size in the middle and corner of a cell (Figure 4) is**
45
46 **optimized with the goal of minimizing the maximum von Mises stress. The optimum values**
47
48 **of these variables are found through a conjugate gradient optimization method, where the**
49
50 **density is set as a constraint.**
51
52
53
54
55
56
57
58

59 **4. Numeric modeling**

1
2
3
4 Both G^1 and G^2 optimum cell geometries have been automatically obtained via in-house Matlab
5
6 (MathWorks, Natick, Massachusetts) subroutines, which have been coupled with ANSYS
7
8 (Canonsburg, Pennsylvania, U.S.A) to build, mesh, and solve the 2D model of the lattice
9
10 material. Assuming in-plane loading conditions, a 2D eight-node element type, Plane 82, with
11
12 plane strain formulation was used since it can model curved boundaries with high accuracy.
13
14 Different combinations of axial and shear loadings are considered to obtain the data required to
15
16 plot the failure surfaces.
17
18

19
20 The effect of the material properties on the normalized fatigue to monotonic strength ratio,
21
22 $\Delta \bar{\tau}_e / \tau_{ult}$, is studied by using aluminum and titanium alloys as bulk properties of the solid
23
24 materials. Aluminum was selected because of its broad application for lightweight foams;
25
26 Titanium is of interest because it is widely used in the aerospace, automobile, sport equipment,
27
28 and biomedical sectors. Table 1 lists the material properties used in this study [66-69]. A bilinear
29
30 elasto-plastic constitutive law was considered to obtain the macroscopic ultimate stress of the
31
32 cellular material. An analysis of the mesh sensitivity (Figure 6) was performed to ensure the
33
34 independency of the results from the mesh size. During this test, the element size of FE model
35
36 was refined, especially around regions of high stress concentration, until the value of the
37
38 maximum stress converged.
39
40
41
42
43
44
45
46
47

48 5. Results

49
50 Figures 7 and 8 show the distribution of von Mises stress (MPa) in the titanium square and
51
52 hexagon with G^1 and G^2 cell boundaries under fully reversed uni-axial and shear loading
53
54 conditions. The stress level significantly changes at the blending points of the G^1 cells, while the
55
56 stress in G^2 cells is distributed uniformly along the cell struts. In addition, it can be seen that
57
58 under uni-axial loading there is no stress concentration at the joints of the G^2 square cell; stress
59
60
61

1
2
3
4 concentration, in fact, occurs at each blending point between an arc and a straight segment, as
5
6 shown in the G^1 unit cell.

7
8 Figure 9 shows the yield (solid marks) and ultimate (open marks) surfaces for both G^1 and G^2
9
10 cells, calculated at relative density of 10%. Here, the geometric parameters of the unit cells were
11
12 selected to optimize the fatigue performance of the lattice under uni-axial and shear loading
13
14 conditions. Figure 9 shows that G^2 cells have higher yield and ultimate strength than those of G^1
15
16 cells. Also, the results show the detrimental effect of the sharp corner, i.e. small-arc fillet radius,
17
18 on the strength of G^1 cells.
19
20
21

22
23 Figure 10 illustrates the effective yield strength of both cells under uni-axial and shear loadings
24
25 as a function of the relative density. As mentioned previously, the values are extracted from the
26
27 intersection of yield/ultimate surfaces with the $\bar{\sigma}_{xx}$ and $\bar{\tau}_{xy}$ axes. Figures 10 (c) and (d) show
28
29 that at low relative densities, the hexagonal G^2 cell has up to 50% higher yield strength in
30
31 comparison to the optimum hexagonal G^1 cell; for higher relative density, on the other hand, the
32
33 two unit cells have comparable yield strength. Figures 10(a) and (b) show that although both
34
35 optimum G^1 and G^2 square lattices have comparable yield strengths under axial loading
36
37 condition, the effect of stress concentration at the joints of the G^1 cell significantly reduces its
38
39 yield strength under shear loading. Table 2 lists the yield/ultimate stresses of the G^1 and G^2 cells
40
41 for different relative densities. Table 3 reports the fatigue to monotonic performance ratio,
42
43 $\Delta \bar{\tau}_e / \tau_{ult}$, of the G^1 and G^2 lattices made of titanium and aluminum 6061T6 alloy [68, 69]. It can
44
45 be observed that the numerical results for conventional lattices with small arc are close to the
46
47 experimental values (0.3 and 0.2 respectively for $R=0.1$ and $R=0.5$) reported by Côté et al [11].
48
49 Furthermore, in agreement with [11], the fatigue to ultimate monotonic stress ratio does not
50
51 depend on the geometry of the unit cell, its relative density, and its material. The conformity of
52
53
54
55
56
57
58
59
60
61
62
63
64
65

1
2
3
4 the results with the experimental data obtained by Côté et al [10, 11] contributes to validate the
5
6 computational-mechanics approach presented in this work.
7

8
9 Figure 11 shows the modified Goodman diagrams of the G^1 and G^2 cells at given relative
10
11 densities, obtained with the values listed in Table 2. The intersection of the diagram with the
12
13 horizontal axis is the ratio of the yield strength of the unit cell to the relative density. The
14
15 corresponding value on the vertical axis is the alternative macroscopic stress, which - as
16
17 described in section 2 - generates a stress level equal to the fatigue endurance limit of the solid
18
19 material.
20
21
22
23
24
25

26 **6. Discussion**

27
28 Figures 7 and 8 show the pivot role that cell shape has on yield, ultimate and fatigue strengths of
29
30 square and hexagon lattices. For each case, stress localization can be observed in G^1 cells with
31
32 sharp corners, an instance that reduces fatigue strength as opposed to what occurs with smooth
33
34 G^2 corners. As shown in Figures 7(a-b) and 8(a-b), the fatigue strength of a regular lattice,
35
36 obtained with G^1 cells with sharp corners, can be substantially improved by optimizing the unit
37
38 cell variables that control the occurrence of stress concentration. For example, Table 2 shows
39
40 that at relative density of 10% optimum square G^1 or G^2 cells have respectively 48.8% and 54%
41
42 higher yield strength (fatigue strength) under fully reverse tension. This and other observations
43
44 are also confirmed for dissimilar relative density by the data in Table 3, which shows the fatigue
45
46 to monotonic performance ratio, $\Delta \bar{\tau}_e / \tau_{ult}$, of the G^1 and G^2 lattices made of Ti-6Al-4V and
47
48 aluminum 6061T6 alloy [68, 69]. In addition, Table 3 shows the results of the unit cells with
49
50 small arc are in good agreement with the experimental values reported by Côté et al [11].
51
52
53
54
55
56

57
58 A comparison between the maximum stress (Figures 7 and 8) and failure surfaces (Figure 9) of
59
60 the optimum G^1 and G^2 cells shows the benefit of a systematic cell shape optimization for fatigue
61
62
63
64
65

1
2
3
4 life. The results show that G^2 cells, especially the hexagonal cell, can distribute more efficiently
5
6 the material within the RVE, thereby lowering the maximum stress and leveling stress
7
8 localization (Figures 7 and 8). Thus, in comparison with G^1 cells, the failure surfaces of G^2 cells
9
10 are wider, showing a higher fatigue resistance.

11
12
13 By comparing the failure surfaces of G^2 and G^1 cells (Figure 9), we notice that the former have a
14
15 higher fatigue resistance for bending dominated lattices. In contrast for the square geometry,
16
17 which is stretching dominated under uni-axial loading, G^2 cells have fatigue resistance
18
19 comparable to G^1 cells. Here, the stress in the cell walls is parallel to the applied load and fairly
20
21 uniform (Figure 7), with maximum value mainly controlled by the thickness of the cell members.
22
23

24
25 Thus, the material distribution around cell joints and the curvature discontinuity at its blending
26
27 points have a minor effect on the stress regime of the lattice. On the other hand for a bending
28
29 dominated lattice, the bending moment at the cell corners is maximum, which indicates that the
30
31 maximum stress and fatigue resistance is controlled by the material distribution in this region.
32
33 Figure 11 shows that an optimized distribution of material at the G^2 cell joints increases the
34
35 fatigue strength of bending dominated lattices, i.e. lattices with hexagonal cells under in-plane
36
37 pure shear and uni-axial loadings, and square cell under in-plane pure shear.
38
39

40
41 As expected, the modified Goodman diagrams of G^2 cells cover a wider range of applied
42
43 alternating/mean stresses in comparison with their G^1 counterparts. It should be noted that figure
44
45 11 shows the modified Goodman of lattices only for uni-axial and pure shear loadings. In
46
47 practice, however, a mechanical component should resist complex load combinations, which
48
49 produce multi-axial macroscopic stress states in each point. Thus for fatigue design, the modified
50
51 Goodman diagrams should be obtained at critical regions subjected to a multi-axial stress state.
52
53

54
55 Figure 9 illustrates the failure surfaces, which are given here for this purpose. For example, for a
56
57 prescribed multi-axial stress state, such as $\sigma_2 = 0.5\sigma_1$ and $\tau = 0$, the distance between the origin
58
59
60

1
2
3
4 and intersection points with the ultimate/yield surfaces can be chosen as yield and ultimate
5
6 stresses to derive the corresponding modified Goodman diagram. Such a methodology can be of
7
8 interest to find the optimized unit cells in a component made of a graded lattice material. In
9
10 addition, the method can be further extended to consider the stress distribution in the unit cells
11
12 close to the material boundaries and to model the effect of the grain size distribution in thin-wall
13
14 cells [40]
15
16
17
18
19
20

21 **7. Conclusion**

22
23 A methodology based on computational mechanics has been presented to design planar lattice
24
25 materials for fatigue failure. Asymptotic homogenization has been used to determine the
26
27 macroscopic yield strength, ultimate strength, and endurance limit, each required to generate the
28
29 modified Goodman diagrams of the lattice. A comparison with the experimental data available in
30
31 literature shows a good agreement of the results.
32
33

34
35 As a case study, the methodology has been applied to investigate the effect of cell shape on the
36
37 fatigue/monotonic strength of lattices with hexagonal and square cells. Failure surfaces of unit
38
39 cells with their respective material distribution within the RVE and with no geometric stress
40
41 concentration have been obtained. The results show that for bending dominated lattices, cells
42
43 with continuous and minimum curvature geometry have superior fatigue performance than cells
44
45 with shape boundaries defined by line and arc primitives. In addition in bending dominated
46
47 lattice materials, unit cells with G^2 minimum curvature should be preferred over cells with arc-
48
49 rounded joints, especially if manufacturability is not a constraint.
50
51
52
53
54
55
56

57 **References**

- 1
2
3
4 [1] N. Fleck, V. Deshpande, M. Ashby, **Micro-architected materials: past, present and**
5 **future, Proceedings of the Royal Society A: Mathematical, Physical and Engineering**
6 **Science, 466 (2010) 2495.**
7
8
9
10
11 [2] A. Vigliotti, D. Pasini, **Linear multiscale analysis and finite element validation of**
12 **stretching and bending dominated lattice materials, Mechanics of Materials, 46 (2012) 57-**
13 **68.**
14
15
16
17
18 [3] T. Schaedler, A. Jacobsen, A. Torrents, A. Sorensen, J. Lian, J. Greer, L. Valdevit, W.
19 **Carter, Ultralight Metallic Microlattices, Science, 334 (2011) 962-965.**
20
21
22
23 [4] R.S. Kumar, D.L. McDowell, **Multifunctional design of two-dimensional cellular**
24 **materials with tailored mesostructure, International Journal of Solids and Structures, 46**
25 **(2009) 2871-2885.**
26
27
28
29
30 [5] L. Mullen, R. Stamp, P. Fox, E. Jones, C. Ngo, C. Sutcliffe, **Selective laser melting: A**
31 **unit cell approach for the manufacture of porous, titanium, bone in-growth constructs,**
32 **suitable for orthopedic applications. II. Randomized structures, Journal of Biomedical**
33 **Materials Research Part B: Applied Biomaterials, 92 (2009) 178-188.**
34
35
36
37
38
39
40 [6] L.J. Gibson, M.F. Ashby, B.A. Harley, **Cellular Materials in Nature and Medicine,**
41 **Cambridge University Press, New York, 2010.**
42
43
44
45 [7] L. Murr, S. Gaytan, F. Medina, H. Lopez, E. Martinez, B. Machado, D. Hernandez, L.
46 **Martinez, M. Lopez, R. Wicker, Next-generation biomedical implants using additive**
47 **manufacturing of complex, cellular and functional mesh arrays, Philosophical Transactions**
48 **of the Royal Society A: Mathematical, Physical and Engineering Sciences, 368 (2010) 1999-**
49 **2032.**
50
51
52
53
54
55
56
57
58
59
60
61
62
63
64
65

- 1
2
3
4 [8] S. Banerjee, A. Bhaskar, The applicability of the effective medium theory to the
5
6 dynamics of cellular beams, *International Journal of Mechanical Sciences*, 51 (2009) 598-
7
8 608.
9
- 10
11 [9] F. Cote, V. Deshpande, N. Fleck, A. Evans, The compressive and shear responses of
12
13 corrugated and diamond lattice materials, *International Journal of Solids and Structures*,
14
15 43 (2006) 6220-6242.
16
17
- 18 [10] F. Côté, N.A. Fleck, V.S. Deshpande, Fatigue performance of sandwich beams with a
19
20 pyramidal core, *International Journal of Fatigue*, 29 (2007) 1402-1412.
21
22
- 23 [11] F. Côté, V.S. Deshpande, N.A. Fleck, Shear fatigue strength of a prismatic diamond
24
25 sandwich core, *Scripta Materialia*, 56 (2007) 585-588.
26
27
- 28 [12] C. Fleck, D. Eifler, Corrosion, fatigue and corrosion fatigue behaviour of metal
29
30 implant materials, especially titanium alloys, *International Journal of Fatigue*, 32 (2010)
31
32 929-935.
33
34
- 35 [13] N. Fleck, X. Qiu, The damage tolerance of elastic-brittle, two-dimensional isotropic
36
37 lattices, *Journal of the Mechanics and Physics of Solids*, 55 (2007) 562-588.
38
39
- 40 [14] N. FLECK, I. QUINTANA-ALONSO, Damage Tolerance of a Sandwich Panel
41
42 Containing a Cracked Square Lattice Core, *Journal of Sandwich Structures and Materials*,
43
44 (2009).
45
46
- 47 [15] A. Wang, D. McDowell, In-plane stiffness and yield strength of periodic metal
48
49 honeycombs, *Journal of Engineering Materials and Technology*, 126 (2004) 137-156.
50
51
- 52 [16] I. Masters, K. Evans, Models for the elastic deformation of honeycombs., *Composite*
53
54 *structures*, 35 (1996) 403-422.
55
56
- 57 [17] M. Schraad, F. Harlow, A multi-field approach to modeling the dynamic response of
58
59 cellular materials, *International Journal of Mechanical Sciences*, 48 (2006) 85-106.
60
61

- 1
2
3
4 [18] S. Banerjee, A. Bhaskar, Free vibration of cellular structures using continuum modes,
5
6 **Journal of Sound and Vibration, 287 (2005) 77-100.**
7
8
9 [19] M. Ruzzene, Vibration and sound radiation of sandwich beams with honeycomb truss
10
11 **core, Journal of Sound and Vibration, 277 (2004) 741-763.**
12
13
14 [20] A. Wang, D. McDowell, Yield surfaces of various periodic metal honeycombs at
15
16 **intermediate relative density, International Journal of Plasticity, 21 (2005) 285-320.**
17
18
19 [21] L.J. Gibson, M.F. Ashby, **Cellular solids: structure and properties, Cambridge**
20
21 **University Press, Cambridge, UK, 1999.**
22
23 [22] M. Kolluri, M. Mukherjee, F. Garcia-Moreno, J. Banhart, U. Ramamurty, Fatigue of a
24
25 **laterally constrained closed cell aluminum foam, Acta Materialia, 56 (2008) 1114-1125.**
26
27
28 [23] N. Kulkarni, H. Mahfuz, S. Jeelani, L.A. Carlsson, Fatigue crack growth and life
29
30 **prediction of foam core sandwich composites under flexural loading, Composite Structures,**
31
32 **59 (2003) 499-505.**
33
34
35 [24] N. Kulkarni, H. Mahfuz, S. Jeelani, L.A. Carlsson, Fatigue failure mechanism and
36
37 **crack growth in foam core sandwich composites under flexural loading, Journal of**
38
39 **reinforced plastics and composites, 23 (2004) 83.**
40
41
42 [25] K. McCullough, N. Fleck, M. Ashby, The stress-life fatigue behaviour of aluminium
43
44 **alloy foams, Fatigue and Fracture of Engineering Materials and Structures, 23 (2000) 199-**
45
46 **208.**
47
48
49 [26] F. Noble, Acoustic emission and fatigue crack growth in rigid polyurethane foam,
50
51 **Journal of Materials Science, 18 (1983) 1827-1835.**
52
53
54 [27] F. Noble, J. Lilley, Fatigue crack growth in polyurethane foam, **Journal of Materials**
55
56 **Science, 16 (1981) 1801-1808.**
57
58
59
60
61
62
63
64
65

- 1
2
3
4 [28] M. Burman, **Fatigue crack initiation and propagation in sandwich structures**, PhD
5 theses. Department of Aeronautics, Royal Institute of Technology, Stockholm, Sweden,
6
7
8 (1998).
9
- 10
11 [29] O. Olurin, K. McCullough, N. Fleck, M. Ashby, **Fatigue crack propagation in**
12 **aluminium alloy foams**, *International Journal of Fatigue*, 23 (2001) 375-382.
13
14
15 [30] K. McCullough, N. Fleck, M. Ashby, **Uniaxial stress-strain behaviour of aluminium**
16 **alloy foams**, *Acta Materialia*, 47 (1999) 2323-2330.
17
18
19 [31] C. Motz, O. Friedl, R. Pippan, **Fatigue crack propagation in cellular metals**,
20 *International Journal of Fatigue*, 27 (2005) 1571-1581.
21
22
23 [32] J.-S. Huang, S.-Y. Liu, **Fatigue of honeycombs under in-plane multiaxial loads**,
24 *Materials Science and Engineering: A*, 308 (2001) 45-52.
25
26
27 [33] J.-S. Huang, S.-Y. Liu, **Fatigue of isotropic open-cell foams under multiaxial loads**,
28 *International Journal of Fatigue*, 23 (2001) 233-240.
29
30
31 [34] J.S. Huang, J.Y. Lin, **Fatigue of cellular materials**, *Acta Materialia*, 44 (1996) 289-296.
32
33
34 [35] A. Simone, L. Gibson, **Effects of solid distribution on the stiffness and strength of**
35 **metallic foams**, *Acta Materialia*, 46 (1998) 2139-2150.
36
37
38 [36] T. Nicholas, J. Zuiker, **On the use of the Goodman diagram for high cycle fatigue**
39 **design**, *International Journal of Fracture*, 80 (1989) 219-235.
40
41
42 [37] A. Dancygier, D. Yankelevsky, A. Nimrod, W. Benson, H. Shibata, K. Tokaji, T.
43 **Ogawa, H. Shiota, Microstructure dependence of fatigue strength and fatigue crack**
44 **propagation in titanium aluminide**, *International Journal of Fatigue*, 18 (1996) 119-125.
45
46
47 [38] G. Lütjering, J. Williams, A. Gysler, **Microstructure and mechanical properties of**
48 **titanium alloys**, *Microstructure and Properties of Materials*, 2 (2000) 1-74.
49
50
51
52
53
54
55
56
57
58
59
60
61
62
63
64
65

- 1
2
3
4 [39] M. Li, F. Guiu, Subcritical fatigue crack growth in alumina--I. Effects of grain size,
5 specimen size and loading mode, *Acta metallurgica et materialia*, 43 (1995) 1859-1869.
6
7
8 [40] O.C. Zienkiewicz, R.L. Taylor, *The finite element method for solid and structural*
9 *mechanics*, Butterworth-Heinemann, Burlington, US, 2005.
10
11
12 [41] M.S.A. Elsayed, D. Pasini, Analysis of the elastostatic specific stiffness of 2D
13 stretching-dominated lattice materials, *Mechanics of Materials*, 42 (2010) 709-725.
14
15
16 [42] L. Gibson, M. Ashby, *Cellular solids: structure and properties*, Cambridge Univ Pr,
17 1999.
18
19
20 [43] R. Kumar, D. McDowell, Generalized continuum modeling of 2-D periodic cellular
21 solids, *International Journal of Solids and Structures*, 41 (2004) 7399-7422.
22
23
24 [44] R.M. Christensen, *Mechanics of cellular and other low-density materials*, *International*
25 *Journal of Solids and Structures*, 37 (2000) 93-104.
26
27
28 [45] J. Chen, M. Huang, Fracture analysis of cellular materials: a strain gradient model,
29 *Journal of the Mechanics and Physics of Solids*, 46 (1998) 789-828.
30
31
32 [46] B. Hassani, E. Hinton, A review of homogenization and topology optimization I I--
33 analytical and numerical solution of homogenization equations, *Computers & Structures*,
34 69 (1998) 719-738.
35
36
37 [47] B. Hassani, E. Hinton, A review of homogenization and topology optimization I--
38 homogenization theory for media with periodic structure, *Computers & Structures*, 69
39 (1998) 707-717.
40
41
42 [48] W.-X. Wang, D. Luo, Y. Takao, K. Kakimoto, New solution method for
43 homogenization analysis and its application to the prediction of macroscopic elastic
44 constants of materials with periodic microstructures, *Computers & Structures*, 84 (2006)
45 991-1001.
46
47
48
49
50
51
52
53
54
55
56
57
58
59
60
61
62
63
64
65

- 1
2
3
4 [49] Z. Fang, W. Sun, J. Tzeng, Asymptotic homogenization and numerical implementation
5
6 to predict the effective mechanical properties for electromagnetic composite conductor,
7
8 **Journal of Composite Materials**, 38 (2004) 1371.
9
- 10
11 [50] E. Andrews, G. Gioux, P. Onck, L. Gibson, Size effects in ductile cellular solids. Part
12
13 **II: experimental results**, **International Journal of Mechanical Sciences**, 43 (2001) 701-713.
14
- 15
16 [51] W. Warren, E. Byskov, Three-fold symmetry restrictions on two-dimensional
17
18 micropolar materials, **European Journal of Mechanics-A/Solids**, 21 (2002) 779-792.
19
- 20
21 [52] A. Vigliotti, D. Pasini, Stiffness and strength of tridimensional periodic lattices,
22
23 **Computer methods in applied mechanics and engineering**, 229–232 (2012) 27-43.
24
- 25
26 [53] S. Hollister, N. Kikuchi, A comparison of homogenization and standard mechanics
27
28 analyses for periodic porous composites, **Computational Mechanics**, 10 (1992) 73-95.
29
- 30
31 [54] J. Guedes, N. Kikuchi, Preprocessing and postprocessing for materials based on the
32
33 homogenization method with adaptive finite element methods, **Computer methods in**
34
35 **applied mechanics and engineering**, 83 (1990) 143-198.
36
- 37
38 [55] S. Jansson, Homogenized nonlinear constitutive properties and local stress
39
40 concentrations for composites with periodic internal structure, **International Journal of**
41
42 **Solids and Structures**, 29 (1992) 2181-2200.
43
- 44
45 [56] K. Matsui, K. Terada, K. Yuge, Two-scale finite element analysis of heterogeneous
46
47 solids with periodic microstructures, **Computers & Structures**, 82 (2004) 593-606.
48
- 49
50 [57] B. Hassani, A direct method to derive the boundary conditions of the homogenization
51
52 equation for symmetric cells, **Communications in numerical methods in engineering**, 12
53
54 (1996) 185-196.
55
- 56
57 [58] R. Cook, D. Malkus, M. Plesha, R. Witt, **Concepts and applications of finite element**
58
59 **analysis**. 2002, in, Wiley, New York.
60
61

- 1
2
3
4 [59] K.J. Bathe, Finite element procedures, Prentice hall Englewood Cliffs, NJ, 1996.
- 5
6 [60] F. Lipperman, M. Ryvkin, M. Fuchs, Design of crack-resistant two-dimensional
7
8 periodic cellular materials, JOURNAL OF MECHANICS OF MATERIALS AND
9
10 STRUCTURES <http://www.jomms.org>, (2009) 441.
- 11
12
13 [61] H. Harders, K. Hupfer, J. Rosler, Influence of cell wall shape and density on the
14
15 mechanical behaviour of 2D foam structures, Acta materialia, 53 (2005) 1335-1345.
- 16
17 [62] S. Banerjee, D. Bhattacharyya, Optimal design of sandwich panels made of wood
18
19 veneer hollow cores, Composites Science and Technology, (2010).
- 20
21
22 [63] E. Masoumi Khalil Abad, S. Arabnejad Khanoki, D. Pasini, SHAPE DESIGN OF
23
24 PERIODIC CELLULAR MATERIALS UNDER CYCLIC LOADING, in: ASME 2011
25
26 International Design Engineering Technical Conferences & Computers and Information in
27
28 Engineering Conference IDETC/CIE 2011, Washington 2011.
- 29
30
31 [64] H. Neuber, Theory of notch stresses: Principles for Exact Calculation of Strength with
32
33 Reference to Structural Form and Material, 2nd ed., United States Atomic Energy
34
35 Commission, Washington, 1961.
- 36
37
38 [65] C.P. Teng, S. Bai, J. Angeles, Shape Synthesis in Mechanical Design., Acta
39
40 Polytechnica, 47 (2008) 56-62.
- 41
42
43 [66] J. Case, L. Chilver, C.T.F. Ross, Strength of Materials and Structures (4th Edition), in,
44
45 Elsevier, 1999.
- 46
47
48 [67] P. Ducheyne, D. Kohn, T. Smith, Fatigue properties of cast and heat treated Ti---6Al---
49
50 4V alloy for anatomic hip prostheses, Biomaterials, 8 (1987) 223-227.
- 51
52
53 [68] T. Nicholas, Tensile testing of materials at high rates of strain, Experimental
54
55 Mechanics, 21 (1981) 177-185.
- 56
57
58 [69] U.S.D.o. Defense, Aluminum and aluminum alloys, US Dept. of Defense, 1966.
- 59
60
61
62
63
64
65

1
2
3
4
5
6
7 **List of Figures and Tables**
8
9

10
11 **Table 1.** Material properties of bulk solid materials
12

13 **Table 2.** Yield and ultimate strength of G^1 and G^2 unit cells for square and hexagonal lattices
14

15
16 **Table 3.** Fatigue to monotonic performance ratio, $\Delta \bar{\tau}_e / \tau_{ult}$, for G^1 and G^2 lattices made of Ti-6Al-4V
17
18 and Al 6061T6 (material properties in Table 1) at given relative densities.
19

20
21 **Figure 1.** Fatigue design diagrams showing the relation between alternating stress and mean stress for a
22
23 number of cycles.
24

25 **Figure 2.** Periodic boundary conditions for a pair of nodes located on the opposite surfaces, A^- and A^+ ,
26
27 of the RVE
28

29
30 **Figure 3.** Flowchart of the design methodology. For a given cell geometry, shape synthesis is coupled
31
32 with computational analysis follow by size optimization. The goal of the first step is to smooth the
33
34 transitions between the geometric primitives defining the cell inner boundaries, thereby reducing stress
35
36 localization. In the second module, the effective strength properties of the lattice are determined through
37
38 asymptotic homogenization theory. The third step involves the cell size optimization to reduce at
39
40 minimum the maximum von Mises stress in the cell wall.
41
42

43 **Figure 4.** Schematic views of: (a) G^1 square unit cell; (b) G^1 hexagonal unit cell
44

45 **Figure 5.** Schematic views of: (a) G^2 continuous square cell; (b) G^2 continuous hexagonal cell; (c)
46
47 Parameterization of the inner profile of a unit cell portion.
48

49
50 **Figure 6.** Mesh sensitivity showing the independency of the results from the mesh size.
51

52 **Figure 7.** Von Mises stress (MPa) distribution in hexagonal (a) and square (b) unit cells made out of Ti-
53
54 6Al-4V. Lattices under fully reversed uni-axial loading, defined by: G^1 cell with small arc (left), optimum
55
56 G^1 cell (middle), and optimum G^2 cell (right).
57
58
59
60
61

1
2
3
4 **Figure 8.** Von Mises stress (MPa) distribution in hexagonal (a) and square (b) unit cells made out of Ti-
5
6 6Al-4V. Lattices under fully reversed pure shear, defined by: G^1 cell with small arc (left), optimum G^1
7
8 cell (middle), and optimum G^2 cell (right).
9

10 **Figure 9.** Yield and ultimate surfaces of Ti-6Al-4V square and hexagonal unit cells for relative density of
11
12 10%. Projection of yield and ultimate surfaces of the G^1 and G^2 square cells in the planes: $\bar{\sigma}_{xx} - \bar{\sigma}_{yy}$ (a),
13
14
15 $\bar{\sigma}_{xx} - \bar{\tau}_{xy}$ (b), $\bar{\sigma}_{xx} - \bar{\sigma}_{yy}$ (c), $\bar{\sigma}_{xx} - \bar{\tau}_{xy}$ (d).
16
17

18 **Figure 10.** Effective yield strength of the square and hexagonal unit cells under uni-axial and shear
19
20 loading as a function of relative density. Yield strength for square unit cell under uni-axial (a) and shear
21
22 loading respectively (b); (c) and (d) pertain to the hexagonal cell.
23
24

25 **Figure 11.** Modified Goodman diagram for Ti-6Al-4V square and hexagonal unit cells at given relative
26
27 densities. G^1 and G^2 square under uni-axial loading (a), and shear loading condition (b); G^1 and G^2
28
29 hexagon under uni-axial loading (c), and shear loading (d).
30
31
32
33
34
35
36
37
38
39
40
41
42
43
44
45
46
47
48
49
50
51
52
53
54
55
56
57
58
59
60
61
62
63
64
65

Table 1. Material properties of bulk solid materials

	Young's Modulus (E_s)	Poisson's ratio (ν)	Yield strength	Ultimate tensile strength	Fatigue endurance limit	Elongation to fracture (%)
Ti-6Al-4V [67, 68]	110 GPa	0.3	901 MPa	984 MPa	486 MPa	8.9
Aluminum 6061 [69, 70]	69 GPa	0.3	276 MPa	310 MPa	158 MPa	12

Table 2**Table 2.** Yield and ultimate strength of G^1 and G^2 unit cells for square and hexagonal lattices.

		$\rho = 10\%$		$\rho = 10\%$		$\rho = 20\%$		$\rho = 20\%$		$\rho = 30\%$		$\rho = 30\%$	
		Uni-axial tension		shear		Uni-axial tension		shear		Uni-axial tension		shear	
		$\bar{\sigma}_y$ (MPa)	$\bar{\sigma}_{ult}$ (MPa)	$\bar{\tau}_y$ (MPa)	$\bar{\tau}_{ult}$ (MPa)	$\bar{\sigma}_y$ (MPa)	$\bar{\sigma}_{ult}$ (MPa)	$\bar{\tau}_y$ (MPa)	$\bar{\tau}_{ult}$ (MPa)	$\bar{\sigma}_y$ (MPa)	$\bar{\sigma}_{ult}$ (MPa)	$\bar{\tau}_y$ (MPa)	$\bar{\tau}_{ult}$ (MPa)
Square unit cell	G^1 cell with Small arc	25.3	49.2	0.519	1.29	46.2	112.4	1.48	3.7	65.4	159.3	3.29	8.5
	Optimum G^1 unit cell	37.65	48.17	0.813	1.5	73	98.4	3.89	7.1	127	138.7	11.3	19.8
	Optimum G^2 unit cell	38.97	43.39	1.26	1.98	77.34	93.4	6.11	9.9	131.7	145.8	15.5	25.3
Hexagonal unit cell	G^1 cell with Small arc	2.29	5.7	1.1	2.56	7.7	21.8	3.78	11.23	17.45	53.18	8	25.6
	Optimum G^1 unit cell	3.68	6.52	1.63	2.9	20.6	40.5	9.63	16	54.2	110.4	25.8	44.7
	Optimum G^2 unit cell	5.48	8.96	2.45	4.25	22.4	44.6	10.4	17.3	56.3	113.86	27.2	47.3

Table 3

Table 3. Fatigue to monotonic performance ratio, $\Delta\bar{\tau}_e / \tau_{ult}$, for G^1 and G^2 lattices made of Ti-6Al-4V and Al 6061T6 (material properties in Table 1) at given relative densities.

		$\rho = 10\%$				$\rho = 20\%$				$\rho = 30\%$			
		$\frac{\Delta\bar{\tau}_e}{\tau_{ult}} (R=0.1)$		$\frac{\Delta\bar{\tau}_e}{\tau_{ult}} (R=0.5)$		$\frac{\Delta\bar{\tau}_e}{\tau_{ult}} (R=0.1)$		$\frac{\Delta\bar{\tau}_e}{\tau_{ult}} (R=0.5)$		$\frac{\Delta\bar{\tau}_e}{\tau_{ult}} (R=0.1)$		$\frac{\Delta\bar{\tau}_e}{\tau_{ult}} (R=0.5)$	
		Al	Ti	Al	Ti	Al	Ti	Al	Ti	Al	Ti	Al	Ti
Square unit cell	G^1 cell with Small arc	0.35	0.34	0.19	0.2	0.3	0.34	0.16	0.2	0.26	0.335	0.14	0.19
	Optimum G^1 unit cell	0.44	0.43	0.26	0.27	0.44	0.44	0.265	0.27	0.445	0.45	0.267	0.29
	Optimum G^2 unit cell	0.48	0.487	0.28	0.318	0.475	0.476	0.28	0.31	0.47	0.474	0.28	0.31
hexagonal unit cell	G^1 cell with Small arc	0.36	0.36	0.2	0.21	0.31	0.3	0.17	0.17	0.28	0.28	0.15	0.156
	Optimum G^1 unit cell	0.45	0.446	0.27	0.282	0.46	0.467	0.278	0.3	0.47	0.45	0.29	0.288
	Optimum G^2 unit cell	0.455	0.45	0.27	0.288	0.46	0.467	0.28	0.3	0.475	0.45	0.29	0.288

Figure 1

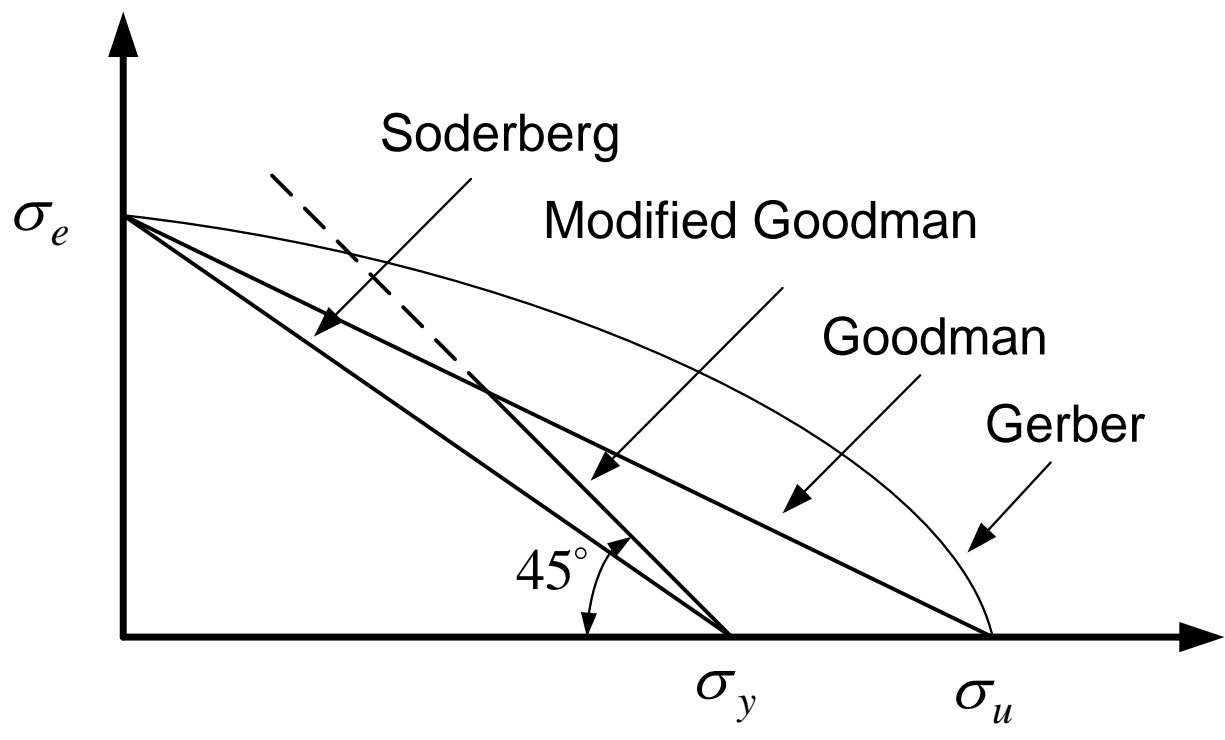


Figure 1. Fatigue design diagrams showing the relation between alternating stress and mean stress for a given number of cycles.

Figure 2

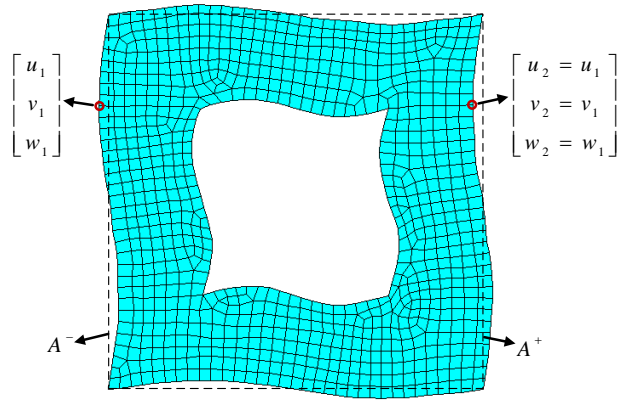


Figure 2. Periodic boundary conditions for a pair of nodes located on the opposite surfaces, A^- and A^+ , of the RVE.

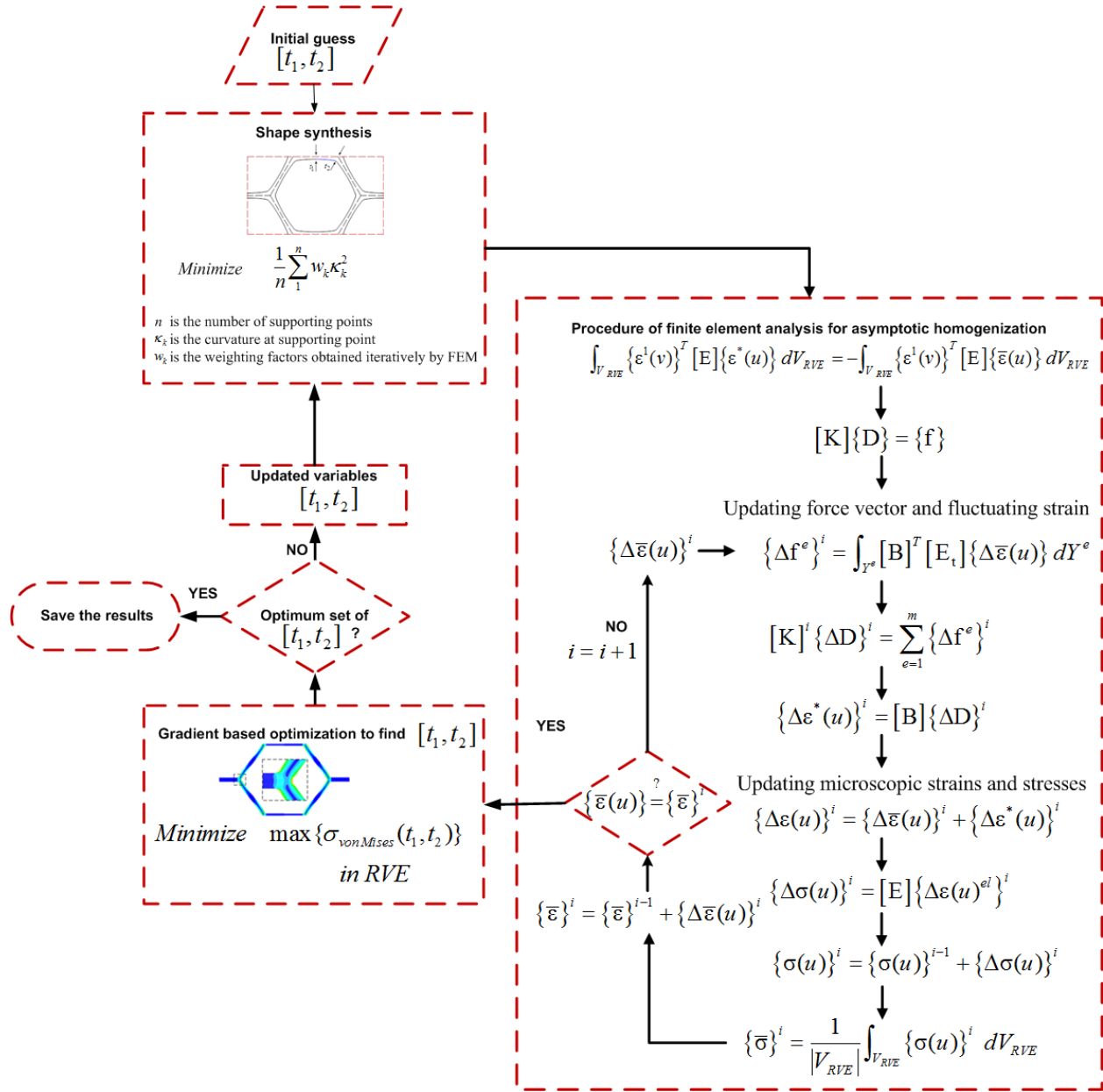


Figure 3. Flowchart of the design methodology. For a given cell geometry, shape synthesis is coupled with computational analysis followed by size optimization. The goal of the first step is to smooth the transitions between the geometric primitives defining the cell inner boundaries, thereby reducing stress localization. In the second module, the effective strength properties of the lattice are determined through asymptotic homogenization theory. The third step involves the cell size optimization to reduce at minimum the maximum von Mises stress in the cell wall.

Figure 4

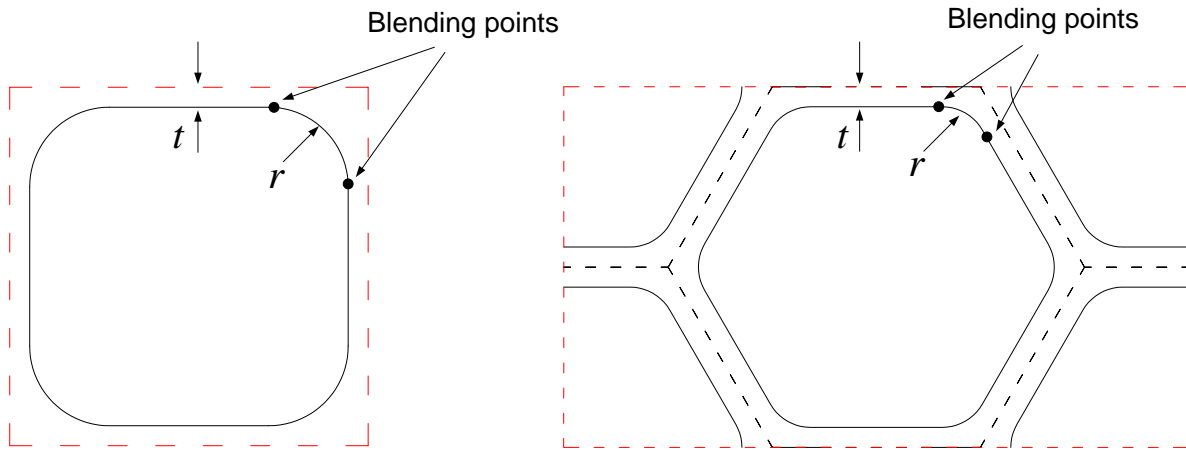


Figure 4. Schematic views of: (a) G^1 square unit cell; (b) G^1 hexagonal unit cell

Figure 5

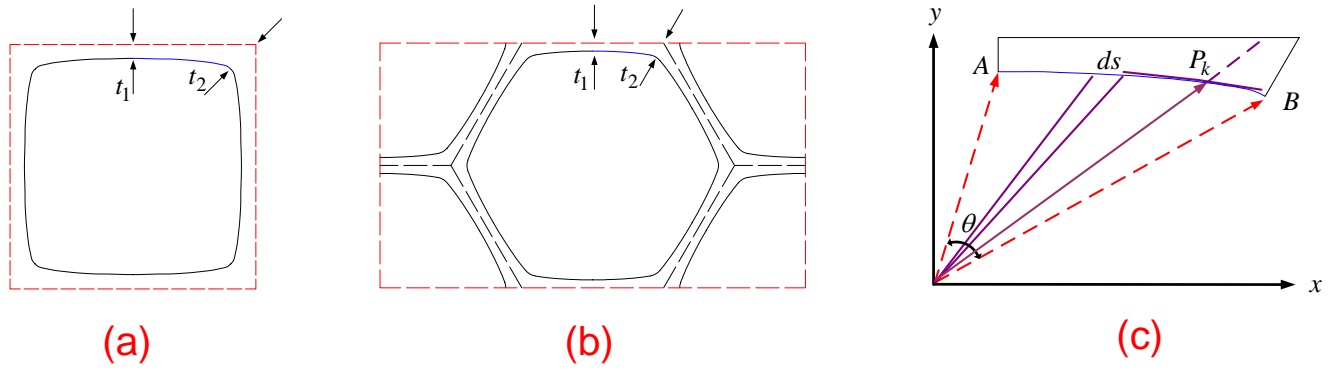


Figure 5. Schematic views of: (a) G^2 continuous square cell; (b) G^2 continuous hexagonal cell; (c) Parameterization of the inner profile of a unit cell portion.

Figure 6

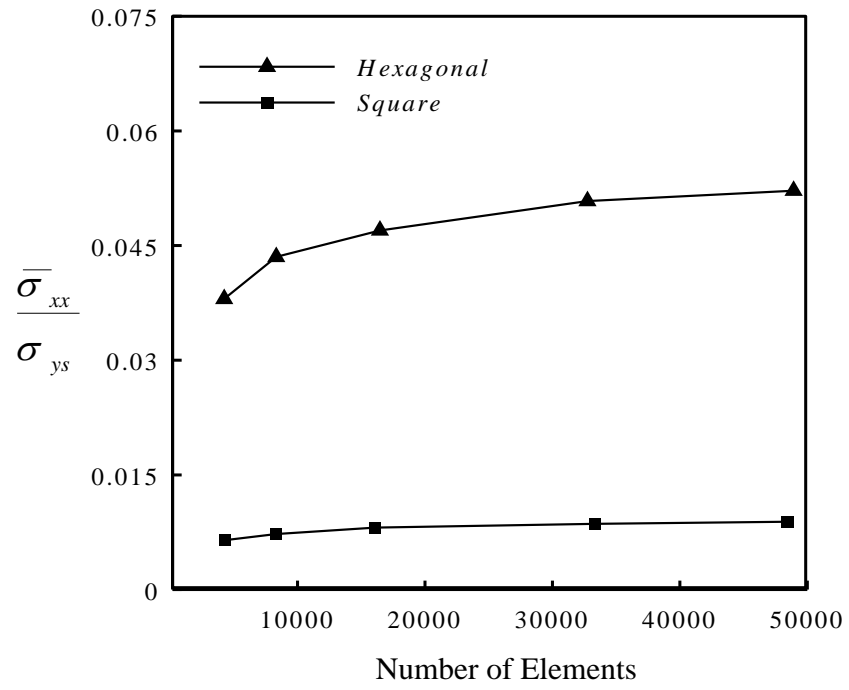


Figure 6. Mesh sensitivity showing the independency of the results from the mesh size.

Figure 7

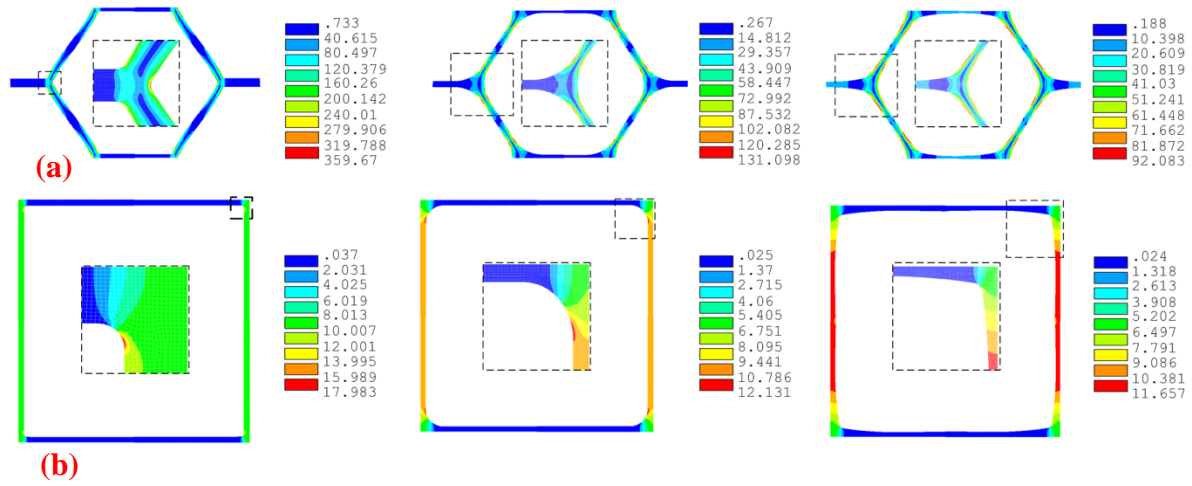


Figure 7. Von Mises stress (MPa) distribution in hexagonal (a) and square (b) unit cells made out of Ti-6Al-4V . Lattices under fully reversed uni-axial loading, defined by: G^1 cell with small arc (left), optimum G^1 cell (middle), and optimum G^2 cell (right).

Figure 8

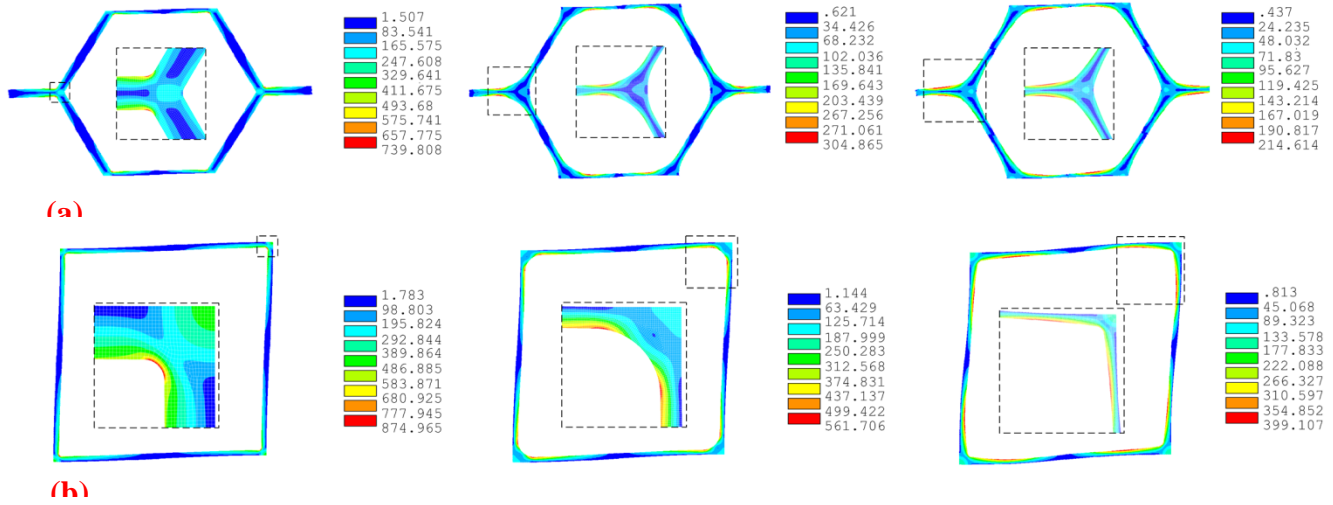


Figure 8. Von Mises stress (MPa) distribution in hexagonal (a) and square (b) unit cells made out of Ti-6Al-4V. Lattices under fully reversed pure shear, defined by: G^1 cell with small arc (left), optimum G^1 cell (middle), and optimum G^2 cell (right).

Figure 9

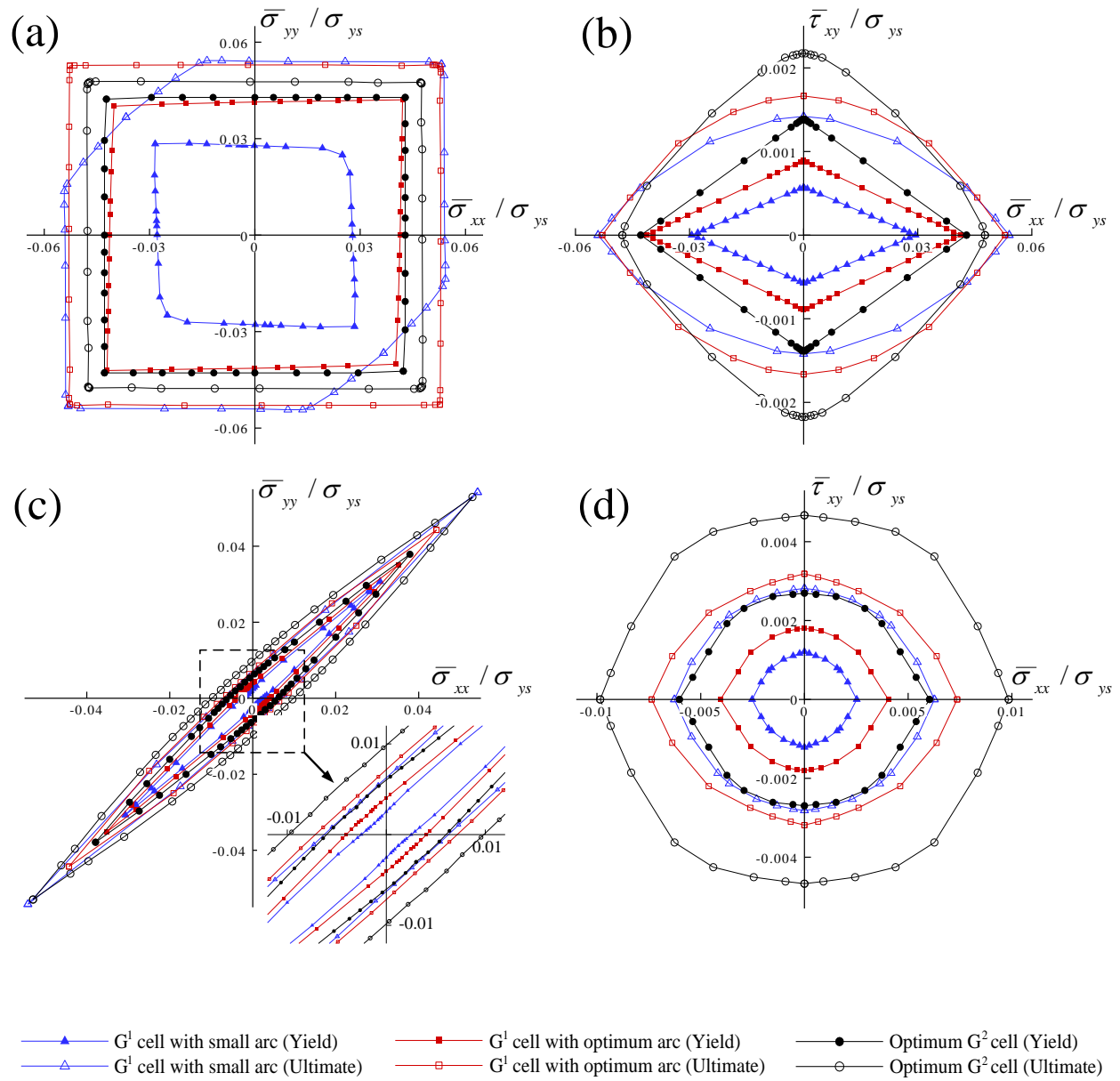


Figure 9. Yield and ultimate surfaces of Ti-6Al-4V square and hexagonal unit cells for relative density of

10%. Projection of yield and ultimate surfaces of G^1 and G^2 square cells in the planes: $\bar{\sigma}_{xx} - \bar{\sigma}_{yy}$ (a),

$\bar{\sigma}_{xx} - \bar{\tau}_{xy}$ (b), $\bar{\sigma}_{xx} - \bar{\sigma}_{yy}$ (c), $\bar{\sigma}_{xx} - \bar{\tau}_{xy}$ (d).

Figure 10

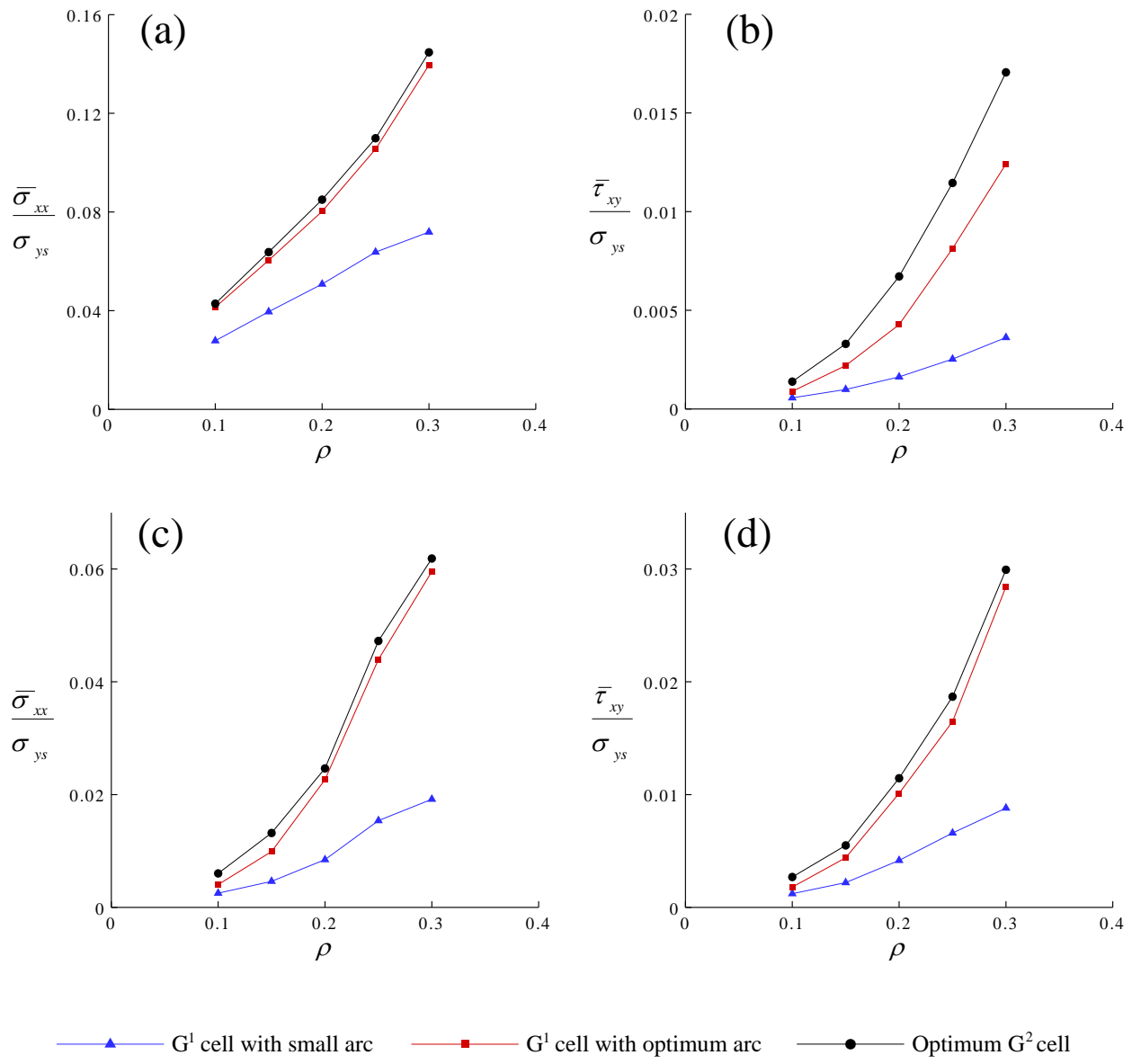


Figure 10. Effective yield strength of the square and hexagonal unit cells under uni-axial and shear loading as a function of relative density. Yield strength for square cell under uni-axial (a) and shear loading respectively (b); (c) and (d) pertain to the hexagonal cell.

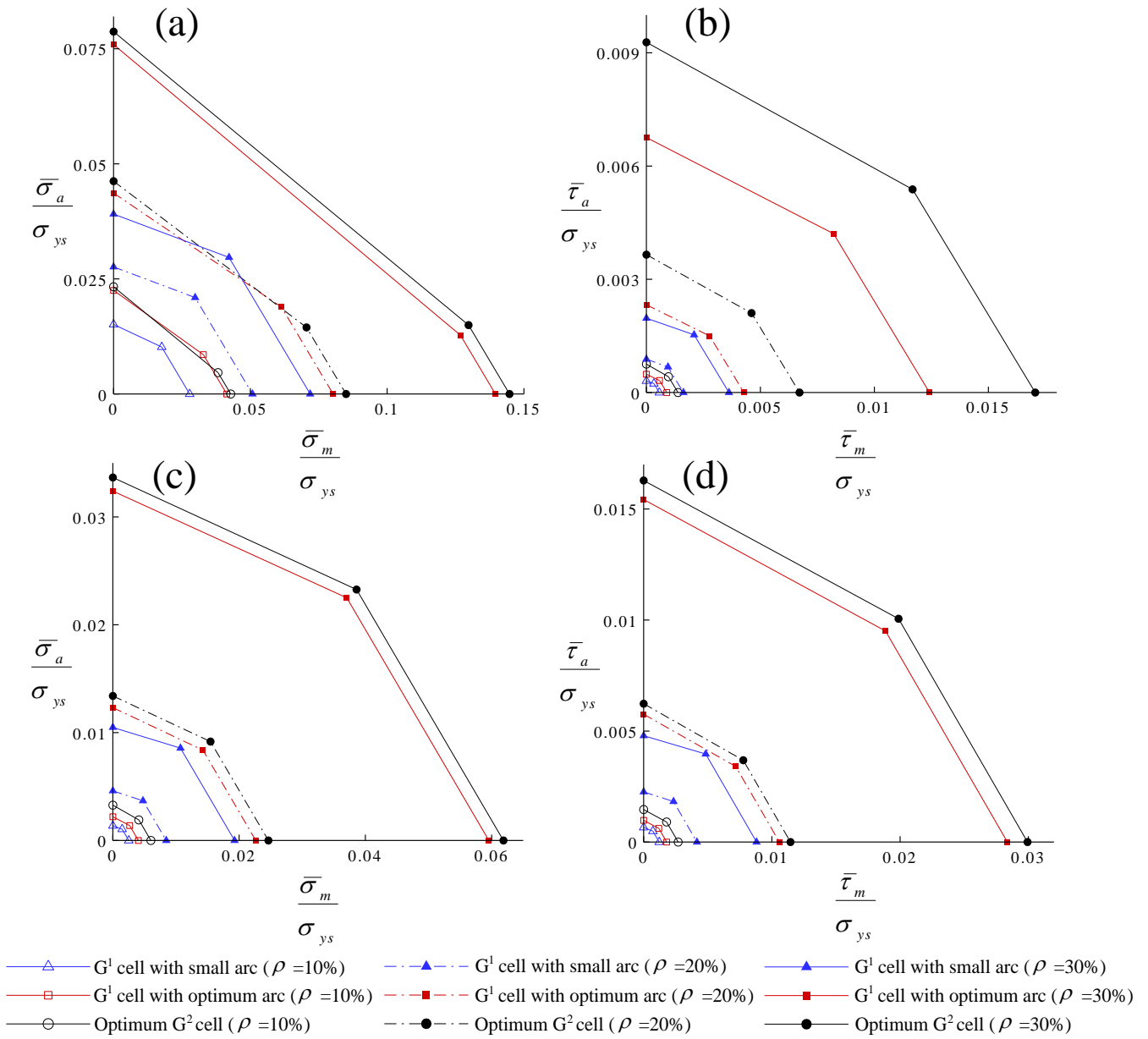


Figure 11. Modified Goodman diagram for Ti-6Al-4V square and hexagonal unit cells at given relative densities. G¹ and G² square under uni-axial loading (a), and shear loading condition (b); G¹ and G² hexagon under uni-axial loading (c), and shear loading (d).